Journal of Applied Electrochemistry **31**: 325–334, 2001.
© 2001 *Kluwer Academic Publishers. Printed in the Netherlands.*

H_2 and H_2/CO oxidation mechanism on Pt/C, Ru/C and Pt–Ru/C electrocatalysts

L. GIORGI[1]*, A. POZIO[1], C. BRACCHINI[1], R. GIORGI[2] and S. TURTÙ[2]
[1]*Electrochemical Energy Conversion Section*
[2]*Materials Technologies and Qualification Section, ENEA, C.R. Casaccia, Via Anguillarese 301, 00060 S. Maria di Galeria, Rome, Italy*
*(*author for correspondence, e-mail: giorgil@casaccia.enea.it, fax: +39 06 30486357)*

Received 13 January 2000; accepted in revised form 26 September 2000

Key words: CO poisoning, electrocatalyst, gas-diffusion electrodes, hydrogen oxidation

Abstract

The oxidation kinetics of H_2 and H_2 + 100 ppm CO were investigated on Pt, Ru and Pt–Ru electrocatalysts supported on a high-surface area carbon powder. The atomic ratios of Pt to Ru were 3, 1 and 0.33. XRD, TEM, EDS and XPS were used to characterize the electrocatalysts. When alloyed with ruthenium, a decrease in mean particle size and a modification of the platinum electronic structure were identified. Impedance measurements in H_2SO_4, at open circuit potential, indicated different mechanisms for hydrogen oxidation on Pt/C (Tafel–Volmer path) and Pt–Ru/C (Heyrowsky–Volmer path). These mechanisms also occur in the presence of CO. Best performances, both in H_2 and H_2 + CO, were achieved by the catalyst with the ratio Pt/Ru = 1. This is due to a compromise between the number of free sites and the presence of adsorbed water on the catalyst. For CO tolerance, an intrinsic mechanism not involving CO electroxidation was proposed. This mechanism derives from changes in the electronic structure of platinum when alloyed with ruthenium.

1. Introduction

Polymer electrolyte fuel cells (PEFCs) are very interesting devices as power systems for electrical vehicles, due to a high power density at low temperatures (70–90 °C). In such types of fuel cell the anode gas-stream is hydrogen rich (also containing CO_2 and CO), produced by reforming or partial oxidation of a hydrocarbon.

The most efficient anode catalyst for hydrogen electrochemical oxidation is nanosized platinum (particles of 2–4 nm) supported on high-surface carbon particles (Pt/C). This catalyst suffers poisoning by the presence of CO, even at low concentrations (10 ppm), in the anode gas stream [1, 2].

Oetjen et al. [3] claim that the behaviour of a PEFC, fed with a H_2/CO mixture at the anode, can be explained by two competing reactions (H_2 and CO adsorption):

$$2\,Pt + H_2 \rightarrow 2\,Pt\text{–}H_{ads} \quad (1a)$$

$$Pt + CO \rightarrow Pt\text{–}CO_{ads} \quad (1b)$$

Therefore, the reduction in PEFC performance can be associated with CO adsorption, which consequently blocks a large number of sites used for the adsorption and oxidation of hydrogen.

The possibility of eliminating adsorbed CO is tied to the following reactions:

$$Pt + H_2O \rightarrow Pt\text{–}OH_{ads} + H^+ + e^- \quad (2)$$

$$Pt\text{–}CO_{ads} + Pt\text{–}OH_{ads} \rightarrow 2\,Pt + CO_2 + H^+ + e^- \quad (3)$$

Platinum does not adsorb water at an electrode potential lower than 0.5 V vs NHE. Reaction 3 takes place at electrode potentials (~0.6 V vs NHE) at which oxygen-containing species are formed on the metal sites. For this reason a Pt anode, which cannot achieve such a potential in an actual PEFC, is a very ineffective electrocatalyst for CO oxidation.

A possible solution to the poisoning problem of the catalyst is the use of a CO-tolerant electrocatalyst. Several authors [3–6] proved that an electrocatalyst obtained by alloying Pt with a second metal M (i.e., Ru, Sn, W etc.) improves the CO tolerance. However, the mechanism responsible for this improvement is not clear. Best performances obtained by Pt–M binary systems could be explained by a promotion effect for the adsorbed CO oxidation, according to a bifunctional mechanism [7].This involves water activation by M and subsequent CO oxidation on neighbouring Pt atoms:

$$M + H_2O \rightarrow M\text{–}OH_{ads} + H^+ + e^- \quad (4)$$

$$Pt\text{–}CO_{ads} + M\text{–}OH_{ads} \rightarrow Pt + M + CO_2 + H^+ + e^- \quad (5)$$

The metal M should supply sites adjacent to platinum for the adsorption of water or oxygenated species. The bifunctional mechanism for the Pt–Ru catalyst was inferred from CO stripping [5], rotating disc electrode [8] and FTIR spectroscopy data [9]. Mass spectrometric studies on porous Pt–Ru catalysts are in agreement with this bifunctional model, predicting that the optimal composition for the oxidation of adsorbed CO should be Pt/Ru = 1 [9].

Nevertheless, further investigations highlighted the limits of such mechanism in the explanation of the CO tolerance. Several authors [7, 8, 10–12] showed that the peak potential for CO stripping on a Pt/Ru = 1 catalyst, was located in the 0.4–0.5 V vs NHE range. Such a range is certainly lower than that of pure platinum, but nevertheless far from the working potential of a PEFC anode [10].

Oetjen et al. [3] analysed the PEFC performance with Pt–Ru anodes fed with a H_2/CO mixture. In their work, at low current density, the alloy Pt/Ru = 1 showed performances similar to that of a Pt catalyst in pure hydrogen; no significant anode overpotential was observed. Therefore, the authors suggested a different mechanism for CO tolerance, which did not involve CO oxidation. Finally, Cooper et al. [10] identified an intrinsic mechanism completely different from the bi-functional one. They used a semi-cell device and analysed the exit gas by means of a mass spectrometer, revealing the presence of CO_2 only at anode potentials higher than 0.3 V vs NHE.

In conclusion, two mechanisms have been hypothesized to explain the CO tolerance of Pt–Ru catalysts. The 'promotion mechanism' (bifunctional model) is based on the promotion of H_2 oxidation by a second metal which catalyses the oxidation of adsorbed CO to CO_2 through H_2O activation; in this way the CO coverage is reduced and the number of active sites for H_2 oxidation is increased. The 'intrinsic mechanism' (electronic model) is based on the idea that the second metal in the catalyst modifies the electronic properties of the pure noble metal. As a consequence, the chemisorption properties of the catalyst, for both H_2 and CO, are also modified so that the CO coverage degree on the sites used for H_2 oxidation is reduced.

At present, the understanding of the exact mechanism remains open to debate: if on one hand the promotion mechanism explains the CO tolerance in a simple way, on the other it does not consider that the working anode potential in an actual PEFC is lower than 0.3 V vs NHE.

The development of an efficient electrocatalyst for PEFC (i.e., with both high catalytic activity for H_2 oxidation reaction and good CO tolerance) is connected to the understanding of the reactive mechanism acting on the electrode. Until today, the best CO-tolerant electrocatalyst seems to be Pt/Ru = 1, which, in typical working conditions of a PEFC [13] at 90 °C, is less active than Pt/C in pure hydrogen and four times more active in H_2 + 100 ppm CO.

Based on these premises, the present work has been focused on the investigation of the H_2 oxidation reaction (HOR) and the CO tolerance mechanism on Pt/C, Ru/C and Pt–Ru/C catalysts.

2. Experimental details

2.1. *Electrodes preparation*

Commercially available Pt, Ru and Pt/Ru (3, 1 and 0.33 Pt/Ru atomic ratio) catalyst powders with the same total metal loading (20 wt %) on carbon black (Vulcan XC72) were obtained from E-TEK.

Three layered (substrate/diffusion layer/catalyst layer) electrodes were prepared using a spray technique [14–16]. The substrate was carbon paper (Toray TGPH090). The ink for the diffusion layer was prepared by mixing appropriate amounts of carbon powder and polytetrafluoroethylene (PTFE 35 wt % dispersion, Hostaflon 5033, Hoechst), as binding agent, with water/isopropyl alcohol at room temperature, under ultrasonic stirring for about 0.5 h. The resulting ink was sprayed over the carbon paper, then thermally treated in air at 70 °C for 0.5 h, at 120 °C for 1 h and at 280 °C for 0.5 h, to remove the solvents and the additives, and sintered at 350 °C for 0.5 h to provide a homogeneous distribution of the polymer. The weight composition of the diffusion layer was 80 wt % of carbon and 20 wt % of PTFE, with a carbon loading of 2.4 mg cm^{-2} and a PTFE loading of 0.6 mg cm^{-2}. Catalyst ink was obtained by mixing proper amounts of the catalyst supported on carbon, Nafion® ionomer (5 wt % solution Aldrich), to bind the catalyst particles and ionic electrolyte, and glycerol (catalyst/Nafion/glycerol = 1.0/0.6/2.5 dry weight ratio) with ethanol at 50 °C under ultrasonic stirring for about 0.5 h. The ink was sprayed on the previously prepared diffusion backing, and then dried in air at 70 °C for 0.5 h. In the Pt and Pt–Ru electrodes, the platinum loading was kept constant at 0.50 mg cm^{-2} and Ru loading was changed according to the Pt/Ru atomic ratio. In the Ru electrode, a metal loading of 0.26 mg cm^{-2} was adopted in order to obtain a Ru concentration equimolar to that of Pt.

2.2. *Microstructure characterization*

X-ray diffraction data were acquired by a powder diffractometer (Philips mod. PW1710) using a CuK_α source. The 2θ angular region between 20° and 140° was explored at a scan rate of 0.025° s^{-1}. Particle dimensions and distribution were obtained by means of a transmission electron microscope (Jeol model 4000-FX). Microanalysis of the Pt–Ru/C catalysts was carried out by using a scanning electron microscopy (Jeol model 8600) with an EDS analyser system (Tracor Northern model 5700).

2.3. *Surface analysis*

XPS measurements were performed by an Escalab MKII V.G. spectrometer. Prior to being analysed, powder catalysts were pressed into a stainless steel sample holder and left one day in the analysis chamber at the base pressure of 10^{-9} mbar, to facilitate residual contamination desorption.

Photoemission spectra from Pt 4f, C 1s, O 1s and Ru 3p levels were taken with non monochromatic AlK_{α} radiation at 1486.6 eV, operating in constant energy analyser mode. The working parameters were a pass energy of 20 eV, which provided a FWHM of 1.2 eV for Ag $3d_{5/2}$ line, and a step size of 0.1 eV.

Peak decomposition was obtained using mixed gaussian/lorentzian curves, after applying background subtraction using the Shirley method.

2.4. *Electrochemical measurements*

The electrochemical measurements were carried out in a conventional three-electrode cell containing 1 M H_2SO_4 electrolyte at 25 °C. The gas diffusion electrode was mounted into a Teflon holder containing a platinum ring current collector and having provision for gas back feeding. The geometric area of the electrode exposed to the electrolyte was 1 cm^2. A flat, large area platinum electrode was used as the counter electrode. A Hg/$HgSO_4$ reference electrode was placed outside the cell. This electrode was connected to the main compartment through a Luggin capillary whose tip was placed as close as possible to the working electrode's surface. The electrochemical cell was connected to a potentiostat/galvanostat (Solartron model 1287) and to a frequency response analyser (Solartron model 1260); both were interfaced with a GPIB card to a personal computer. Electrochemical impedance spectroscopy (EIS) measurements were carried out in H_2 and H_2 + 100 ppm CO, in the frequency range 20 kHz to 0.05 Hz (the amplitude of the ac signal being always 10 mV_{pp}) at open circuit potential (OCP).

Cyclic voltammetry and CO stripping voltammetry were carried out in the same cell configuration described above; however the gas back feeding to the diffusion electrode was excluded. Data were acquired with a potentiostat/galvanostat (EG&G model 273A) interfaced with a GPIB card to a personal computer. The three-electrode cell was purged with argon for 10 min. Ten consecutive cyclic voltammetries (sweep rate 10 mV s^{-1}) were then performed in the potential range 1000–25 mV vs NHE to verify the surface cleanliness and reproducibility. Pure CO was bubbled into the electrolyte for five min and then its adsorption on the electrode was driven under potential control at 25 mV vs NHE for 3 min. The electrolyte was purged for 5 min with argon, maintaining the electrode potential at 25 mV vs NHE, to eliminate the CO, which had reversibly adsorbed on the surface. Anodic sweep from 400 to 1000 mV was performed (sweep rate 20 mV s^{-1}) to electroxidate the irreversibly adsorbed CO. Finally, a cyclic voltammogram was recorded from 1000 mV to 25 mV in order to verify the completeness of the CO oxidation.

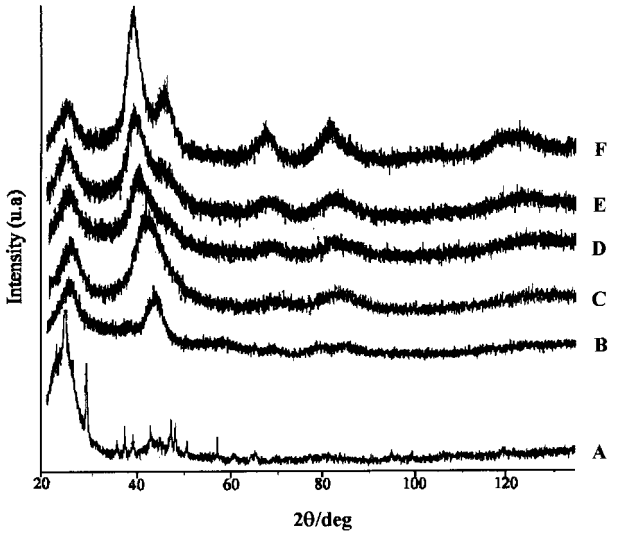

Fig. 1. XRD patterns of carbon (A), Ru/C (B), Pt–Ru/C (1:3 C, 1:1 D, 3:1 E) and Pt/C (F) powders.

3. Results

3.1. *Microstructure characterization*

The X-ray diffraction patterns of Pt/C, Pt–Ru/C, Ru/C and carbon powder (Vulcan XC-72) are compared in Figure 1. Carbon paper shows the C(002) reflection of graphite. The diffraction spectrum of the carbon paper contributes in terms of a linear background in the angular region considered. The Pt/C catalyst exhibits the diffraction peaks of the Pt f.c.c. structure; the Ru/C catalyst exhibits the diffraction peaks of the Ru hcp structure. In the XRD spectra of Pt–Ru/C the angular position of the Pt(111) reflection is shifted towards higher values as Ru content increases. This suggests the formation of Pt–Ru alloy and the progressive decrease of lattice parameter as Ru is increased. When Pt/Ru = 0.33, the alloy is in the two-phase region (f.c.c. + h.c.p.) [39].

The mean particle size obtained from TEM measurements d_m (Å) are shown in Table 1, which also reports the specific surface area ($m^2\ g^{-1}$) calculated according to [16]:

Table 1. Mean particle size (d_m) and surface area (A_s) of different catalysts from TEM data

Catalyst Me/C	d_m /Å	A_s /$m^2\ g^{-1}$
Pt	26	107
Pt/Ru = 3	19	156
Pt/Ru = 1	21	150
Pt/Ru = 0.33	20	169
Ru	21	174

Table 2. Pt/Ru atomic ratios of catalysts in the gas-diffusion electrodes from EDS analysis

Nominal Pt/Ru	Pt/Ru from EDS
3	2.7
1	0.8
0.33	0.30

$$A_s = \frac{60\,000}{\rho d_m} \tag{6}$$

where the catalyst density ρ(g cm^{-3}), has been obtained through the following relation: $\rho_{Pt-Ru} = X_{Pt}\rho_{Pt} + X_{Ru}\rho_{Ru}$ (X is the metal fraction in the alloy). A particle size reduction is observed in the binary catalysts.

The results of the EDS microanalysis of the gas-diffusion electrodes (Table 2) agree with the nominal composition of the alloys.

3.2. *XPS surface analysis*

Catalyst powders Pt/C, Ru/C and Pt–Ru/C with different atomic ratios (Pt/Ru = 0.33, 1, 3) and the reference Pt were analysed by XPS, to study electronic structure and chemical environment. The whole set of measurements was repeated several times at both short and long time intervals.

Photoemission spectra of Pt 4f doublets are reported in Figure 2 for a representative run of measurements. A positive energy shift of 0.3 ± 0.1 eV, with respect to reference Pt bulk was observed for the Pt/C catalyst, according to literature data. Most of the reported experimental data show core level positive shifts in small metal clusters supported on insulating or semimetallic substrates. These shifts have been interpreted either as predominantly due to photoemission final state effects [18–20] or as dominated by initial state effects, electronic reconfiguration of surface atoms and interaction with the substrate [21, 22].

Further slight displacement to higher binding energies of about 0.2–0.3 eV (±0.1 eV) was noticed for all Ru containing samples, regardless of the Pt/Ru atomic ratio. This last shift is unlikely due to the occurrence of different platinum–oxygen interactions in the binary catalysts compared to Pt/C. The reason for this is that the Pt line shape and peak decomposition is the same for both mono- and bimetallic samples. In fact, by curve fitting, the Pt 4f doublet was decomposed into three components: a main component ascribed to Pt^0 at the lowest binding energy; a second one, shifted about 0.8 eV attributed to Pt^{2+}; and a third one, at about 2.7 eV higher than the previous peak due to Pt^{4+} signals. Neither relative intensity nor energy separation of the various components changed between the Pt/C and the binary catalysts, indicating the same Pt–O interaction.

Contrary to what other authors have claimed [23], a possible reason for the larger positive shift of bimetallic samples is that the Pt electronic structure is modified by the presence of Ru. The sign of the resulting shift would be in agreement with the work of McBreen and Mukerjee [23], who found, by XAS measurements, that Ru increases vacancies in the Pt valence band, leading to more tightly bound electrons in core levels. The same conclusions were derived by TPD and TPR measurements [25].

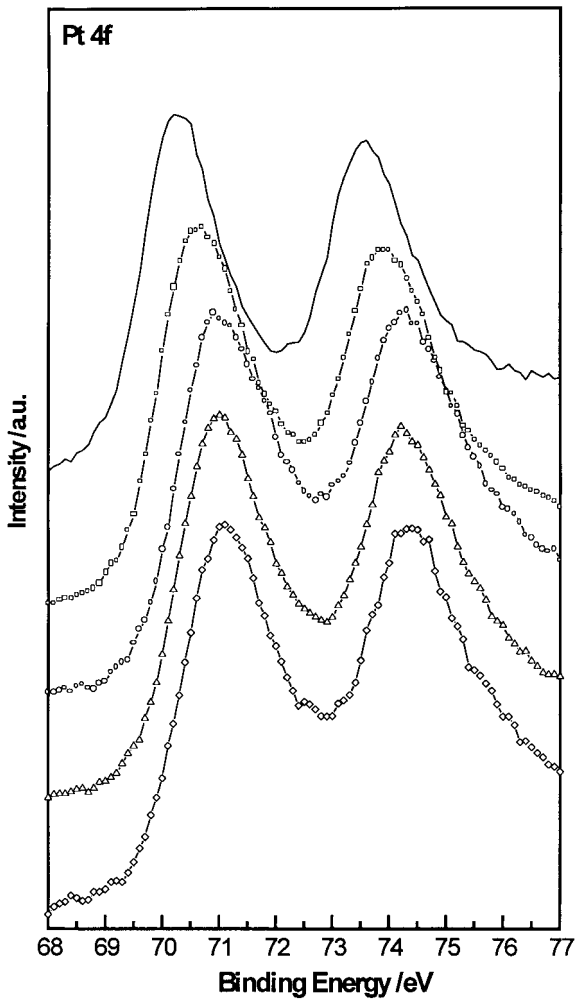

Fig. 2. XPS Pt 4f spectra of Pt bulk (solid line), nanometric Pt/C (square symbol) and Pt–Ru/C catalysts with different composition (3:1 circle symbol, 1:1 triangle symbol, 1:3 diamond symbol).

The less intense Ru $3p_{3/2}$ was recorded due to the overlapping of the predominant Ru photoemission line, Ru 2p, with the carbon peak. Small shifts of this line were also observed (Figure 3), but they were not unambiguously correlated to alloying effects. This is not surprising since these peaks are rather large and asymmetric for two reasons. First, line width is influenced by the contribution of nonstoichiometric oxides and weak bonds with oxygen-containing groups. Second, peaks have an asymmetric shape induced by the tail at about 464 eV, attributed to very low signals from stoichiometric oxides.

In addition, from the O 1s spectra reported in Figure 4, it can be seen that two different interactions with oxygen take place. On the one hand, spectra

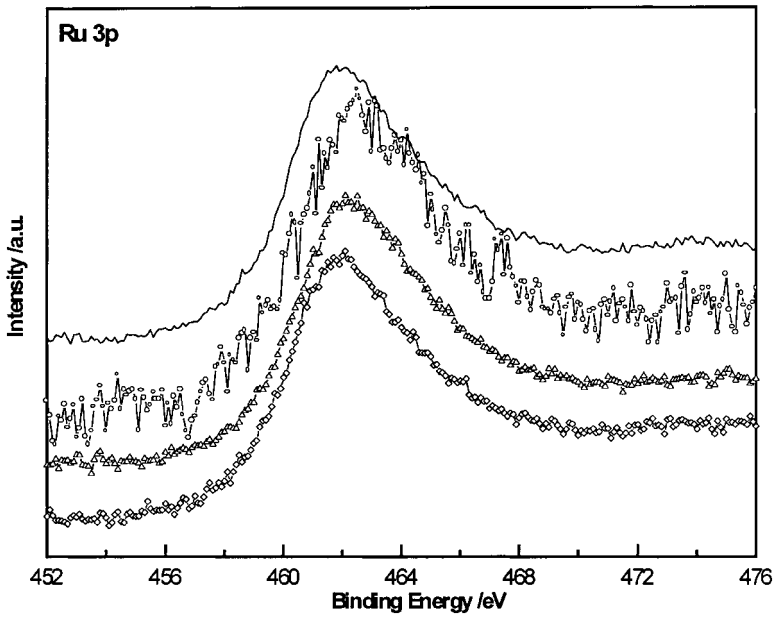

Fig. 3. XPS Ru 3p spectra of nanometric Ru/C (solid line) and Pt–Ru/C catalysts with different composition (3:1 circle symbol, 1:1 triangle symbol, 1:3 diamond symbol).

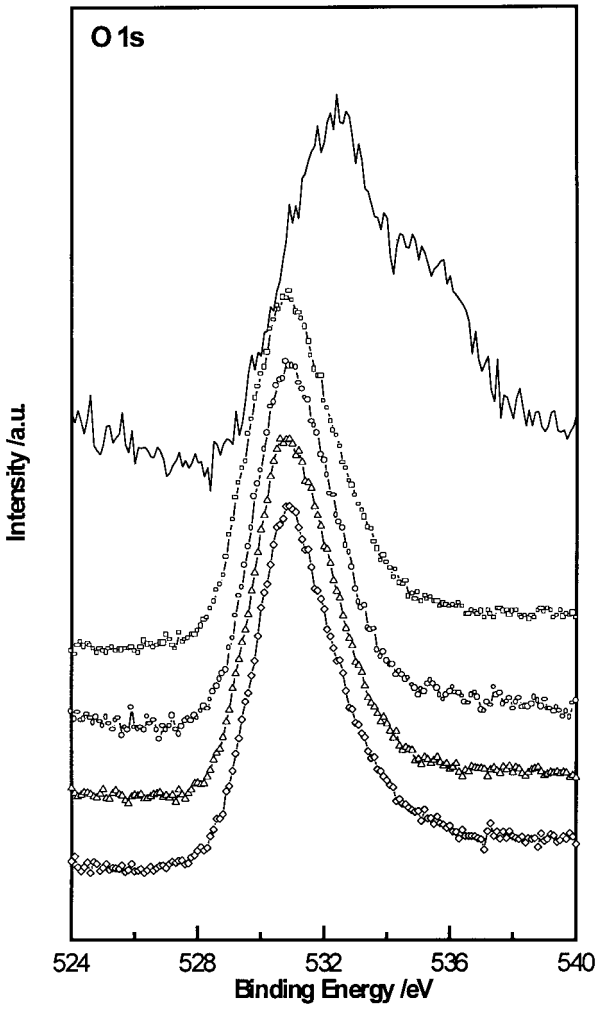

Fig. 4. XPS O 1s spectra of nanometric Pt/C (solid line), Ru/C (square symbol) and Pt–Ru/C catalysts with different composition (3:1 circle symbol, 1:1 triangle symbol, 1:3 diamond symbol).

relative to Ru/C and Pt–Ru/C showed a main line at about 530.5 eV, which is typical of oxide and hydroxide bonds. On the other hand, the Pt/C catalyst exhibited the major component centred in the range of contamination species (C=O bond at ~532 eV and water at ~535 eV). A constant intensity of these contributions could not be reproduced for each time interval, due to its random nature.

3.3. *Hydrogen oxidation reaction and influence of ruthenium content*

Impedance data for Pt/C and Pt–Ru/C catalysts, at OCP in pure H_2, with constant platinum loading and different amounts of ruthenium in the Pt–Ru alloys are shown in Figure 5. The observed semicircle can be ascribed to the hydrogen oxidation reaction (HOR) on the catalytic sites, and its diameter represents the polarization resistance, R_p, (charge transfer, diffusion and adsorption). The R_p increased in the following order: Pt < Pt–Ru $\ll$ Ru. Among the Pt–Ru/C catalysts, the R_p order was: (Pt/Ru = 1) < (Pt/Ru = 0.33) < (Pt/Ru = 3).

Polarization resistance of the Pt/C catalyst was 10–20 times lower than Pt–Ru/C alloys, while the Ru/C polarization resistance was 20–30 times higher than for Pt–Ru/C alloys and 350 times higher than for Pt/C.

All impedance data have been fitted using Boukamp's software [14]. Many equivalent circuits were tested to individualise three fundamental models. Figures 6 and 7 show the three equivalent circuit models used for the different catalysts, the experimental data and the related best-fit results. The models were in good agreement with the experimental data and permitted a quantitative analysis to estimate different phenomena acting on the catalysts. The best fit circuit for Pt/C (Figure 6(a)) was a

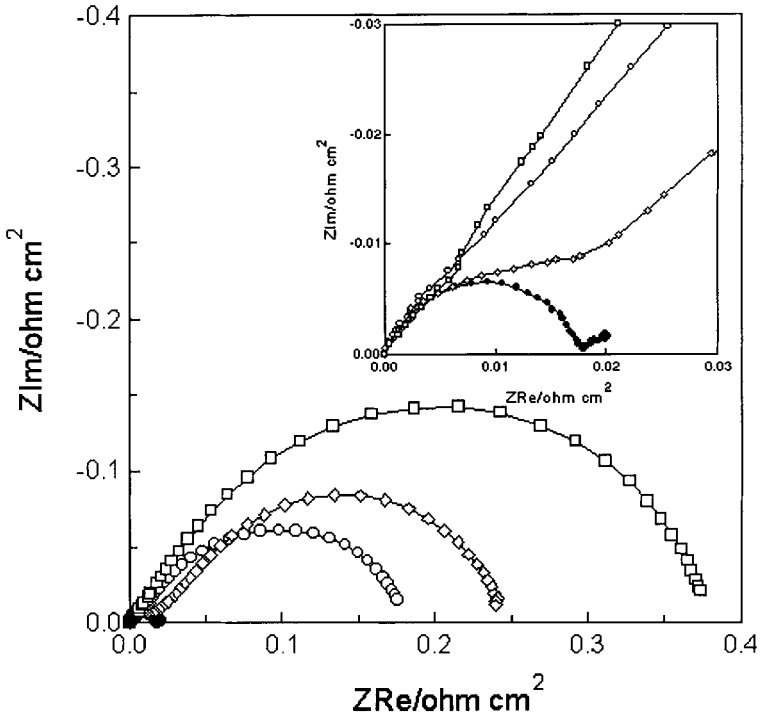

Fig. 5. Impedance diagrams of Pt/C (black square symbol) and Pt–Ru/C gas-diffusion electrodes at OCP with hydrogen gas feeding (H_2SO_4 1 M, 25 °C), with different amount of ruthenium in the alloy (3:1 square symbol, 1:1 circle symbol, 1:3 diamond symbol). Insert shows detail of high frequencies region.

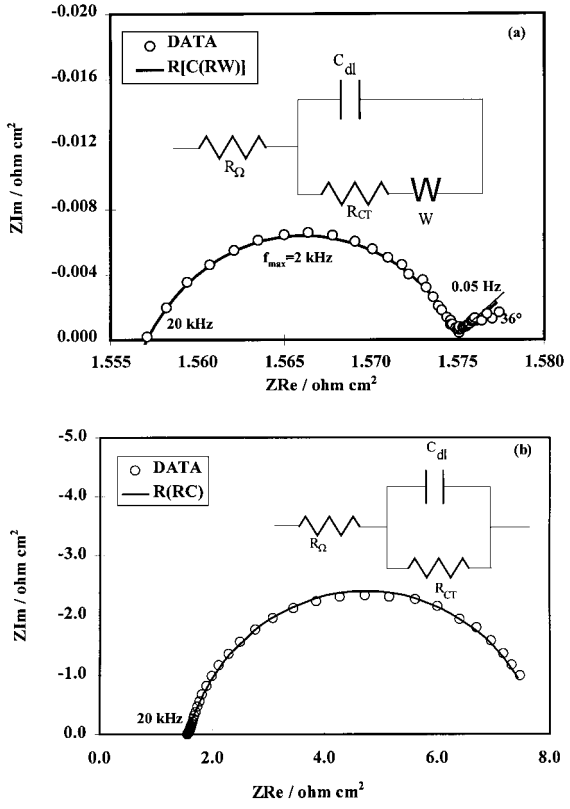

Fig. 6. Impedance diagrams of Pt/C (a) and Ru/C (b) gas-diffusion electrode at OCP with hydrogen gas feeding (H_2SO_4 1 M, 25 °C). Experimental data (○) fitted (—) with the displayed equivalent circuit.

Randles circuit, characteristic for single-step charge transfer processes limited by a diffusion phenomena. This model includes an external ohmic resistance, R_Ω, a charge transfer resistance, R_{ct}, a double layer capacitance, C_{dl}, and a Warburg, W, diffusion element.

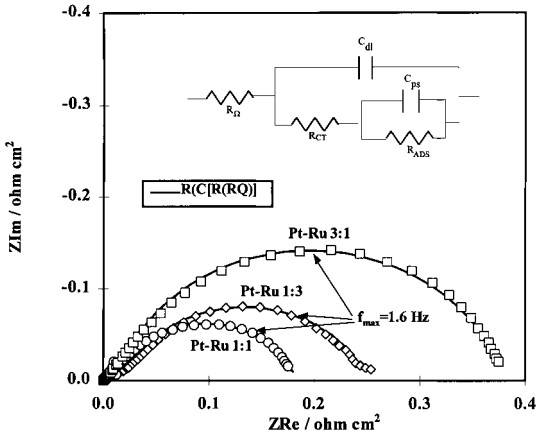

Fig. 7. Impedance diagrams of Pt–Ru/C gas-diffusion electrode at OCP in hydrogen (H_2SO_4 1 M, 25 °C). Experimental data (○) were fitted (—) with the displayed equivalent circuit.

To check the validity of the curve fit, some parameters were calculated by means of circuit elements to verify their physical meaning. Therefore, the exchange current density i_o for the Pt/C obtained from R_{ct} was 1×10^{-3} A cm^{-2}, in agreement with literature data. Taking into account the contribution from carbon support, the electrochemical active surface (EAS) calculated from C_{dl} [27] was 83 m^2 g^{-1}, which was in agreement with TEM data (Table 1). By means of the Warburg element, the product $CD^{0.5}$ (4.7×10^{-8} mol cm^{-2} s$^{-0.5}$) was calculated, where D and C are, respectively, the diffusion coefficient and the concentration of H_2. The

same parameter $CD^{0.5}$, calculated from literature data [28] for hydrogen in 0.5 M sulphuric acid at 25 °C, is 4.4×10^{-9} mol cm^{-2} s$^{-0.5}$.

The circuit model for Ru/C (Figure 6(b)) is very similar to the Pt/C one but without the presence of the Warburg element. The exchange current density i_o was 100 times lower than that of Pt/C (9×10^{-6} A cm^{-2}), indicating a slow hydrogen oxidation reaction. The same conclusion was reported by Gasteiger et al. [38] by means of the RDE technique. Also for the Ru/C, the EAS obtained from double layer capacitance (161 m^2 g^{-1}) was in agreement with TEM data.

The equivalent circuit, used for data fitting of Pt–Ru/C catalysts (Figure 7) is characteristic of the electrical response of an electrochemical reaction with a strongly adsorbed intermediate. The model includes the same elements as the Ru/C catalyst (R_Ω, R_{ct} and C_{dl}) and two new ones: the adsorption pseudocapacitance C_{ps} and the adsorption resistance R_{ads}. These two terms respectively contain the contribution of the surface concentration (coverage) of the adsorbed intermediates and the rate of adsorption/desorption. The results of the fittings are shown in Table 3.

Exchange current density (i_o from R_{ct}) of all Pt–Ru/C catalysts was of the same order of magnitude as that of the Pt/C catalyst ($\sim 10^{-3}$ A cm^{-2}). Considering the polarization resistance R_p as the sum of charge transfer and adsorption resistance, the changes in R_p values were totally ascribed to the adsorption resistance R_{ads}. As reported by Conway et al. [29] an adsorption pseudocapacitance is usually 10–100 times higher than the double layer capacitance. The value of C_{ps} from our EIS data was found to be 10–20 times higher than double layer capacitance values.

Considering the components of the circuit models, two time constants were found, related to two different processes: charge transfer $R_{ct}C_{dl}$ and adsorption $R_{ads}C_{ps}$. However, only Pt–Ru/C also showed the $R_{ads}C_{ps}$ time constant, which referred to an adsorption process in the low frequencies range. The order of magnitude for the reactive RC time constant was 1200 times higher than the adsorption one. This second phenomenon was attributed to to the presence of Ru, which probably involves oxygenated species (H_2O, OH^-) adsorbed on ruthenium sites, as reported by other authors [30, 31]. Figure 8 shows the C_{ps} and R_{ads} trend for all the Pt–Ru/C catalysts. The lowest R_{ads} and highest C_{ps} was found for Pt–Ru/C catalysts with an atomic ratio Pt/Ru = 1.

Table 3. Results of the fitting, by using the equivalent electrical circuit of Figure 7, for the hydrogen oxidation on Pt–Ru electrocatalysts

Catalyst Me/C	C_{dl} /μF cm^{-2}	R_{ct} /mΩ cm^2	C_{ps} /μF cm^{-2}	R_{ads} /mΩ cm^2
Pt/Ru = 3	35 ± 12	18 ± 4	562 ± 15	363 ± 6
Pt/Ru = 1	56 ± 13	14 ± 2	1400 ± 46	170 ± 3
Pt/Ru = 0.33	40 ± 8	24 ± 5	1040 ± 39	213 ± 4

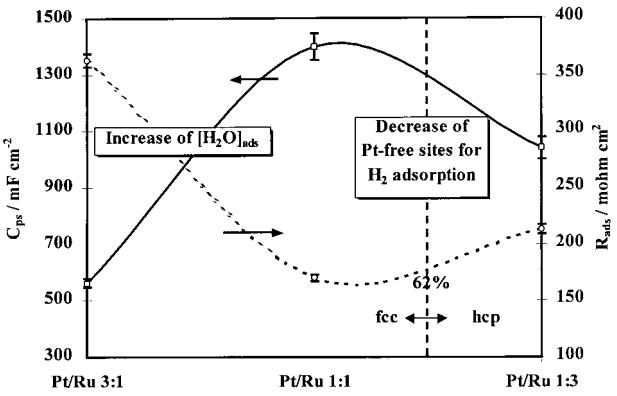

Fig. 8. Adsorption pseudoresistance and pseudocapacitance of Pt–Ru/C catalyst as a function of Pt/Ru ratio.

3.4. *Influence of CO poisoning on hydrogen oxidation reaction*

Polarization resistance against time for all catalysts in H_2 + 100 ppm CO at OCP is shown in Figure 9. After 150 min, the R_p of Pt/C and Ru/C had a value an order of magnitude higher than Pt–Ru/C alloys. On the one hand, polarization resistance of Pt/C catalysts increased 800 times in only 180 min, showing that the CO adsorption is a fast process, while the R_p of Ru/C maintained a constant value. On the other hand, the R_p of Pt–Ru/C catalysts increased 2–3 times the initial values for all samples, showing a good tolerance of Pt–Ru alloy to CO poisoning. Figure 10 shows the R_p values as a function of the Ru atomic fraction, both at the beginning of the experiments and after 164 min, with flowing gas H_2 + 100 ppm CO. The trend observed for R_p in the presence of CO was the same as that observed in pure H_2: (Pt/Ru = 1) < (Pt/Ru = 0.33) < (Pt/Ru = 3). Catalysts with atomic ratios of Pt/Ru = 1 yielded the best performance.

The CO stripping voltammetry on the Pt/C catalyst showed the CO oxidation peak at 0.83 V vs NHE. In the

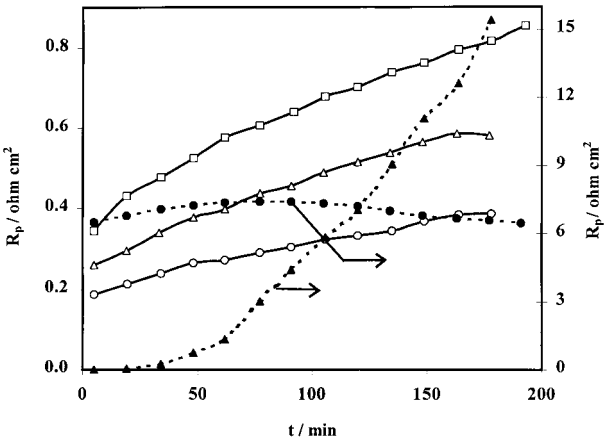

Fig. 9. Polarisation resistance against time for Pt/C (triangle filled symbol), Ru/C (circle filled symbol) and Pt–Ru/C (1:3 triangle open symbol, 1:1 circle open symbol, 3:1 square open symbol) gas-diffusion electrodes fed with H_2 + 100 ppm CO at OCP (H_2SO_4 1 M, 25 °C).

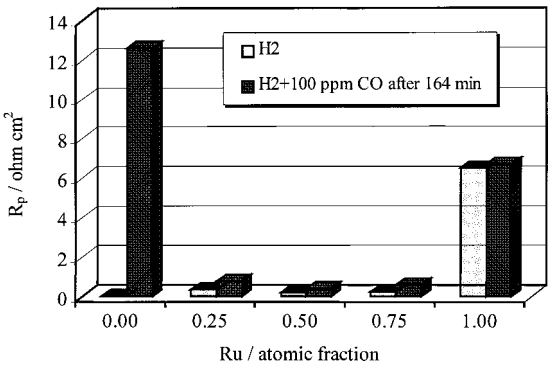

Fig. 10. Comparison of polarization resistance of Pt/C, Ru/C and Pt–Ru/C in H_2 and H_2 + 100 ppm CO.

case of Pt–Ru/C catalysts, the CO oxidation peaks are located in the potential range 0.67–0.83 V. The increase of ruthenium in the catalyst layer produced a shift of CO oxidation peaks, towards lower potential (Figure 11).

4. Discussion and conclusions

4.1. *Hydrogen oxidation reaction (HOR)*

In pure hydrogen the NLLS equivalent circuit obtained for Pt/C (Figure 6(a)) describes a single-step charge transfer process with a diffusive phenomenon at low frequencies (Randles circuit). The experimental data were in agreement with the Tafel–Volmer mechanism [32] for H_2 oxidation (Figure 12(a)). The reaction mechanism was of the CE type (chemical adsorption + discharge):

$$2\,Pt + H_2 \rightarrow 2\,Pt\text{–}H_{ads} \quad \text{(Tafel)} \tag{7a}$$

$$Pt\text{–}H_{ads} + H_2O \rightarrow Pt + H_3O^+ + e^- \quad \text{(Volmer)} \tag{7b}$$

The alloying of platinum with ruthenium modifies the electronic properties of Pt and introduces into the HOR a different intermediate step with strongly adsorbed oxygenated species. The equivalent circuit (Figure 6(b)) suggests a different mechanism for HOR, on Pt–Ru/C

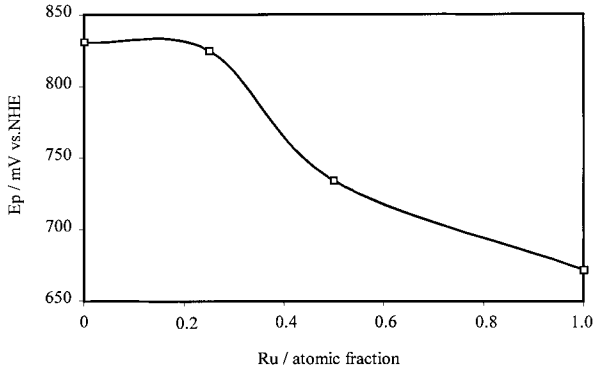

Fig. 11. Influence of the ruthenium content in the Pt–Ru alloy on the CO oxidation peak of the cyclic voltammetry.

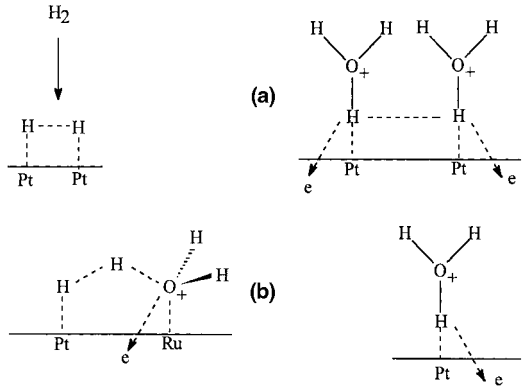

Fig. 12. Hydrogen oxidation mechanism on Pt/C (a) and Pt–Ru/C (b) electrocatalyst.

catalysts, based on the Heyrowski–Volmer path [33] (Figure 12(b)). The reaction mechanism is of the CEE type (chemical adsorption + electrochemical adsorption + discharge):

$$Pt + H_2 \rightarrow Pt\text{–}H_{2ads} \qquad Ru + H_2O \rightarrow Ru\text{–}H_2O_{ads} \tag{8a}$$

$$Pt\text{–}H_{2ads} + Ru\text{–}H_2O_{ads} \rightarrow Pt\text{–}H_{ads} + Ru + H_3O^+ + e^- \quad \text{(Heyrowski)} \tag{8b}$$

$$Pt\text{–}H_{ads} + H_2O \rightarrow Pt + H_3O^+ + e^- \quad \text{(Volmer)} \tag{8c}$$

In the Pt–Ru alloys, the Ru atoms attract water molecules and hold them more strongly than the surrounding surface Pt atoms. The Ru atoms may be able to hold and orient H_2O molecules, perhaps disrupting hydrogen bonded molecules, so that they can dissociate.

The best performance of the Pt/Ru = 1 catalyst for the HOR is related to the Heyrowski–Volmer mechanism. In fact, two different contributions act when the Ru atomic fraction decreases in the alloy (Figure 8): (i) the decrease of adsorbed H_2O on Ru sites, as also shown by our XPS data (Figure 4) and confirmed by ASED–MO calculations [34]; (ii) the increase of free Pt atoms for H_2 adsorption. This last effect takes place when the Ru content increases and the crystallographic structure changes from f.c.c. to f.c.c. + h.c.p. [39]. In the latter

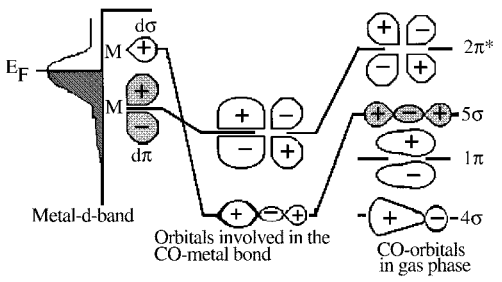

Fig. 13. Influence of ruthenium in the Pt–Ru alloys on the CO–Pt adsorption bond.

structure, the Pt atoms are closely packed and are not free for H_2 adsorption. Therefore, the best HOR performance of Pt/Ru = 1 alloy is related to a compromise between these effects: number of free Pt sites and presence of adsorbed H_2O.

4.2. *CO poisoning*

Although CO poisoning does not seem to influence Ru/C catalyst, it is a fast process on the Pt/C catalyst (Figure 9). CO poisoning of Pt–Ru alloys is strongly limited by the presence of ruthenium atoms. The performance of Pt–Ru alloys in H_2 + CO always shows the same trend as in pure H_2 with a maximum for Pt/Ru = 1. As was demonstrated in the discussion about the behaviour in pure hydrogen, this optimum ratio is related to the H_2 oxidation mechanism (Heyrowski–Volmer path, Equation 8), rather than to the bifunctional CO oxidation mechanism (Equation 5).

In agreement with other authors [10, 24, 25], an intrinsic mechanism, which does not involve CO oxidation, was hypothesized; in fact, all impedance data were collected at OCP, therefore well below the onset of CO oxidation to CO_2. Furthermore, our cyclic voltammetry measurements on Pt–Ru catalysts showed the CO oxidation peak at potentials (0.67–0.83 V vs NHE), very far from the hydrogen oxidation region (0.0–0.3 V vs NHE).

According to the Blyholder model [35], the adsorption of CO on platinum can be explained by two simultaneous bond stabilization effects (Figure 13): (i) electronic transfer from the filled 5σ-orbital of CO to the empty d-band of platinum; (ii) backdonation of electrons from metal dπ to the empty $2\pi^*$ antibonding orbital of CO (Figure 13). This bonding mechanism is synergetic, since the drift of metal electrons into CO orbitals will tend to make the CO molecule entirely negative and hence increase its basicity via the σ orbital of carbon. At the same time, the drift of electrons to the metal tends to make the CO positive, thus enhancing the acceptor strength of the π orbital [36, 37].

A change that would tend to inhibit the shift of electrons from metal to CO π orbitals, such as placing a positive charge on the metal, should lead to a weaker CO–metal bond. The Ru presence induces such modifications by changing the electron density of states N(E), with a shift of the Fermi energy level with respect to CO orbital energy. This decreases the backdonation effect with an inhibition of the electron shift from metal to CO π orbitals. As a consequence, the Pt–CO synergetic bonding mechanism looses its stabilization effect.

In agreement with these considerations, Bautier et al. [25] reported that an increase in CO tolerance of Pt–Ru could be at least partially explained by the reduced CO adsorption energy. This is caused by an electronic modification of Pt atoms, due to the interaction with the neighbouring Ru atoms. Rodriguez [37] reported that the heat of adsorption for CO on a metal should be inversely proportional to the separation between the centroid of the metal d-band and the CO ($2\pi^*$) orbital. As already mentioned, this phenomenon was highlighted by McBreen et al. [24] by XAS data; they concluded that alloying with Ru causes an increase in the number of Pt d-band vacancies. The XPS data obtained (Figure 2) agree with this hypothesis. In fact, in the alloys , the increase of the Pt core levels binding energy can be interpreted as arising from changes in the electronic density of the d-band.

5. Conclusions

In conclusion, the following considerations can be drawn:

(i) hydrogen oxidation reaction (HOR) proceeds with different mechanisms on Pt/C and Pt–Ru/C catalysts;
(ii) the presence of ruthenium in the alloy catalyst modifies the electronic structure of the platinum and introduces a different intermediate step in HOR, with strongly adsorbed oxygenated species;
(iii) Tafel–Volmer mechanism for HOR on the Pt/C catalyst was confirmed, while a Heyrowski–Volmer mechanism on Pt–Ru/C catalysts is proposed;
(iv) CO poisoning of catalysts is partially limited by the presence of ruthenium in catalyst alloys;
(v) the performance of Pt–Ru/C catalysts in the presence of CO shows the same trend as in pure hydrogen;
(vi) the observed difference of performance among the Pt–Ru/C catalysts appear to be related to HOR mechanisms and do not involve CO oxidation; and
(vii) a CO tolerance intrinsic mechanism for Pt–Ru/C catalysts was postulated: ruthenium atoms, at every atomic fraction, modify the electronic properties of platinum, thus reducing CO adsorption.

Acknowledgements

The authors would like to acknowledge E-TEK, Inc. (Natik, MA, USA) for supplying the catalyst powders and to thank Dr M. Angiolini (ENEA) for TEM analysis.

References

1. Proceedings of a workshop on 'The Electrocatalysis of Fuel Cell Reactions', 15–16 May 1978, New York, p. 169.
2. S. Gottesfeld and J. Pafford, *J. Electrochem. Soc.* **135** (1988) 2651.
3. H.F. Oetjen, V.M. Schnidt, U. Stimming and F. Trila, *J. Electrochem. Soc.* **143** (1996) 3838.
4. A. Gasteiger, N. Markovic, P.N. Ross and E.J. Cairns, *J. Phys. Chem.* **98** (1994) 617.
5. A. Gasteiger, N. Markovic and P.N. Ross, *J. Phys. Chem.* **99** (1995) 16 757.
6. Proceedings 49th Annual Meeting of International Society of Electrochemistry, 13–18 Sept. 1999, Kitakyushu, Japan.
7. M. Watanabe and S. Motao, *J. Electroanal. Chem.* **60** (1975) 267.

8. T.J. Schmidt, H.A. Gasteiger and R.I. Behm, *J. Electrochem. Soc.* **146** (1999) 1296.
9. R. Ianiello, V.M. Schmidt, V. Stimming, J. Stumper and A. Waller, *Electrochim. Acta* **146** (1994) 1863.
10. S.J. Cooper, A.G. Gunner, G. Hoogers and D. Thompsett, Proceedings 2nd International Symposium on 'New Materials for Fuel Cell and Modern Battery System', 6–10 July 1997, Montreal, Canada, p. 286.
11. R. Ianiello, V.M. Schmidt, J.L. Rodriguez and E. Pastor, *J. Electroanal. Chem.* **471** (1999) 167.
12. Z. Jusys and H. Baltruschat, Proceedings 1997 ISE/ECS Joint Int. Meeting, 31 Aug.–5 Sept. 1998, Paris, p. 1045.
13. A. Pozio, L. Giorgi, E. Antolini and E. Passalacqua, Proceedings 1998 ISE/ECS Joint Int. Meeting, 31 Aug.–5 Sept. 1997, Paris, abstract 505.
14. L. Giorgi, E. Antolini and A. Pozio, *Electrochim. Acta* **43** (1996) 3675.
15. E. Antolini, L. Giorgi, A. Pozio and E. Passalacqua, *J. Power Sources* **77** (1999) 136.
16. F. Lufrano, E. Passalacqua, G. Squadrito, A. Patti and L. Giorgi, *J. Appl. Electrochem.* **29** (1999) 445.
17. P. Stonehart and G. Kohlmayr, *Electrochim. Acta* **17** (1972) 369.
18. G.K. Wertheim, S.B. Di Cenzo and S.E. Youngquist, *Phys. Rev. Lett.* **51** (1983) 2310.
19. P.H. Citrin and G.K. Wertheim, *Phys. Rev. B* **27** (1983) 3176.
20. S.B. Di Cenzo and G.K. Wertheim, *J. Electron Spectrosc. Relat. Phenom.* **43** (1987) C7.
21. F. Parmigiani, E. Kay, P.S. Bagus and C.J. Nelin, *J. Electron Spectrosc. Relat. Phenom.* **36** (1981) 257.
22. P.S. Bagus, C.J. Nelin, E. Kay and F. Parmigiani, *J. Electron Spectrosc. Relat. Phenom.* **43** (1987) C13.
23. A.K. Shukla, A.S. Aric, K.M. El-Kathib, H. Kim, P.L. Antonucci and V. Antonucci, *Appl. Surf. Sci.* **137** (1999) 20.
24. J. McBreen and S. Mukerjee, *J. Electrochem. Soc.* **142** (1995) 3399.
25. F. Bautie de Mongeot, M. Scherer, B. Gleich, E. Kopatzki and R.J. Behm, *Surf. Sci.* **411** (1998) 249.
26. B.B. Boukamp, Report CT88/265/128, University of Twente, The Netherlands (1988).
27. L. Giorgi, A. Pozio and C. Bracchini, GEI98 – Giornate dell'Elettrochimica Italiana 1998, 23–26 Sept. 1998, Bologna, Italy.
28. L.G. Austin and S. Almaula, *J. Electrochem. Soc.* **114** (1967) 926.
29. B.E. Conway, V. Birss and J. Wojtowicz, *J. Power Source* **66** (1997) 1.
30. H.A. Gasteiger, N. Markovic, P.N. Ross Jr. and E.J. Cairns, *J. Electrochem. Soc.* **141** (1994) 1795.
31. E. Ticianelli, J.B. Beery, M.T. Paffet and S. Gottesfeld, *J. Electroanal. Chem.* **258** (1989) 61.
32. J.O'M. Bockris, 'Surface Electrochemistry', (Plenum Press, New York, 1993).
33. D. Galizzioli, F. Tantardini and S. Trasatti, *J. Appl. Electrochem.* **5** (1975) 203.
34. A.B. Anderson, E. Grantscharova and S. Seong, *J. Electrochem. Soc.* **143** (1996) 2075.
35. B. Beden, C. Lamy, N.R. de Tacconi and A.J. Arvia, *Electrochim. Acta* **35** (1990) 691.
36. F.A. Cotton and G.W. Wilkinson, '*Advanced Inorganic Chemistry*' (Interscience, New York, 1966).
37. J.A. Rodriguez, *Surf. Sci. Rep.* **24** (1996) 223.
38. H.A. Gasteiger, N. Markovic and P.N. Ross Jr., *J. Phys. Chem.* **99** (1995) 8290.
39. F. Richard, B. Wohlmann, U. Vogel, H. Hoffschulz and K. Wandelt, *Surf. Sci.* **335** (1995) 361.